Table 3 Multivariate analysis of the predictive factors for incidence of hepatocellular carcinoma in all 382 patients

Factors	Hazard ratio	95% CI	*P* value
Virological response			
SVR	1		
Non-SVR	8.413	1.068–66.300	0.043
AFP integration value			
<10	1		
≥10	2.580	0.999–6.659	0.050

SVR sustained virological response, *IFN* interferon, *AFP* alpha-fetoprotein

Table 4 Multivariate analysis of predictive factors for incidence of hepatocellular carcinoma in 197 non-SVR patients

Factors	Hazard ratio	95% CI	*P* value
AFP integration value			
<10	1		
≥10	4.039	1.570–10.392	0.004
Sex			
Female	1		
Male	3.636	1.383–9.563	0.009

AFP alpha-fetoprotein

(HR 3.636, 95% CI 1.383–9.563, $P = 0.009$) (Table 4). There was no significant difference in other variables including those identified as predictive factors in the entire study population (i.e., age, non-SBR, ALT integration value, AFP before interferon therapy) (Table 2).

AFP integration value as a predictive factor for HCC

Further analysis focused on the AFP integration value as this was the strongest predictive factor for incidence of HCC in non-SVR patients. Of the 382 patients, both baseline and AFP integration values were available for 321. These were divided into four groups: (1) AFP "low–low," (2) AFP "low–high," (3) AFP "high–low," and (4) AFP "high–high," for baseline AFP-average AFP integration values, respectively, where "high" is ≥10 ng/mL and "low" is <10 ng/mL. As shown in Fig. 3a, of the 321 patients, 211 (65.7%) showed baseline AFP levels <10 ng/mL. Of these 211, 207 (98%), were in the AFP low–low group, and only four in the AFP low–high groups. Baseline characteristics, including age, gender, serum HCV-RNA, aspartate aminotransferase (AST), ALT, bilirubin, white blood cell, hemoglobin, platelet, observation periods, and number of times of AFP measurement, were not different between AFP high–low group and high–high group. However, AFP-low group, which is a combination of the low–high and low–low groups, showed significantly lower AST level ($P < 0.00001$), lower ALT level ($P < 0.00001$), higher platelet count ($P < 0.00001$), shorter observation period ($P = 0.01448$), and fewer number of times of AFP examination ($P = 0.00035$), compared to both AFP high–high and AFP high–low group. Six patients (2.8%) with baseline AFP levels <10 ng/mL developed HCC in the follow-up period and none of these patients were among the four low–high group patients. Even in patients with high baseline AFP levels, incidence of HCC was only 3.9% among the AFP high–low group (2 of 51 patients). In contrast, 20.3% of patients in the AFP high–high group developed HCC during the follow-up period.

The incidence rate of HCC in three patient groups, "AFP-low" (a combination of the "low–high" and "low–low" groups),"high–low," and "high–high", was estimated using the Kaplan–Meier method and compared using log-rank tests (Fig. 3b). The rate of HCC incidence was significantly higher in the AFP high–high group compared to both the AFP high–low group and patients with low baseline AFP levels ($P = 0.009$ and 0.001, respectively). There was no significant difference between patients with low baseline AFP levels and the AFP high–low group. The 7-year incidence rate of HCC was 32.3% in the AFP high–high group, compared to only 6.6% in the AFP high–low group, and 8.1% in all patients with low pre-treatment levels.

Discussion

It is well recognized that the most effective strategy for the prevention of HCC development in patients with chronic hepatitis C is likely to be the complete elimination of the HCV infection accompanied by the resultant normalization of liver function [7, 12, 13, 15, 16, 19]. Indeed, we confirmed here that non-SVR is the most significant predictive factor for incidence of HCC in patients receiving interferon therapy for chronic hepatitis C. However, it should be noted that the risk of HCC, even in non-SVR patients, differs between individuals. In the current study, we identified AFP integration value and male gender as independent risk factors for incidence of HCC in non-SVR patients. The incidence of HCC was significantly reduced in individuals with average AFP integration values < 10 ng/mL after interferon therapy, which suggests that the decrease of AFP by interferon therapy lowers the risk of developing HCC. Indeed, even where patients had high baseline AFP levels, incidence of HCC was reduced when the AFP integration value decreased after interferon therapy. Thus, our current findings identify AFP integration value as a useful predictive marker of HCC development in non-SVR patients.

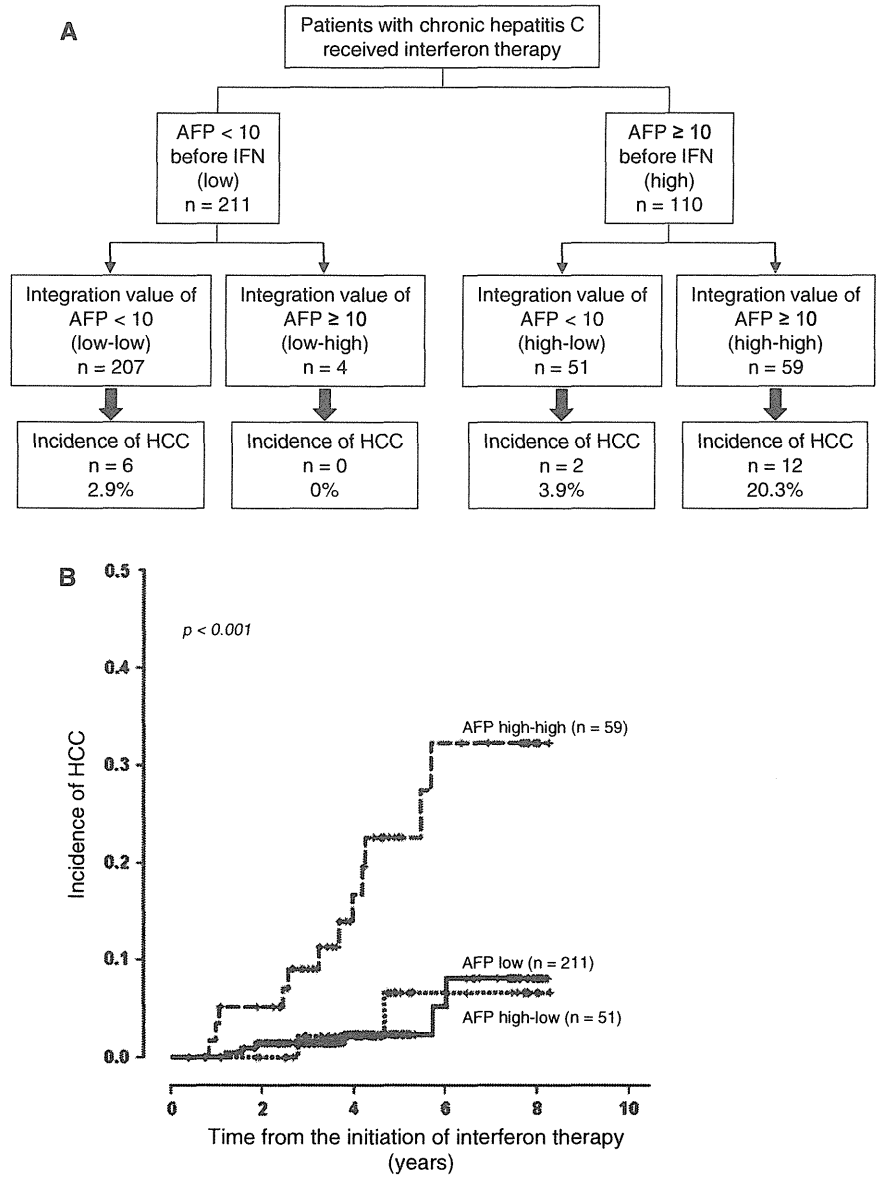

Fig. 3 AFP integration value as a predictive factor for HCC. **a** *Flow diagram* showing the number of patients (*n*) classified by baseline alpha-fetoprotein (AFP) levels before interferon (IFN) therapy and average AFP integration value, and the incidence of hepatocellular carcinoma (HCC) of each group. **b** Kaplan–Meier estimates of the incidence of HCC. *Solid line* AFP-low group (AFP levels before interferon therapy <10 ng/mL); *dotted line* AFP high–low group (baseline AFP levels ≥10 ng/mL, average AFP integration value <10 ng/mL); *dashed line* AFP high–high group (both baseline and average AFP integration values ≥10 ng/mL)

Data from several previous studies suggest that the continuous normalization of alanine aminotransferase (ALT) levels by interferon therapy can reduce the risk of HCC development [36–39]. In addition, one recent study suggested that the ALT integration value is a predictive factor for HCC [35]. In contrast to published data (22), our multivariate analysis did not identify the ALT integration value as a significant predictive factor for HCC incidence, although it was identified as significant by univariate analysis in all 382 patients. Since the previous study did not evaluate AFP levels as a factor for prediction of HCC [35], our results indicate that the AFP integration value is superior to that of ALT as a predictive factor for incidence of HCC. We do not know the reason for this result, but it is speculated that significance of AFP as a marker of hepatic regeneration resulted in the more accurate prediction of hepatocarcinogenesis by integration value of AFP than that of ALT.

As AFP is a diagnostic marker for the existence of HCC, high integration value of AFP in the present study might be a result of HCC development. However, we concluded that the high AFP integration values in patients who developed HCC were not caused by a result of existence of HCC, because of the following two reasons. First, the last AFP values before detection of HCC were not the highest level in the follow-up periods in 19 of 23 patients who developed

HCC, suggesting that the AFP was not produced by the developing HCC in these patients. Second, to exclude the influence of the remaining four patients whose last AFP levels were the highest in the follow-up periods, we analyzed the same statistical analysis by using average AFP integration values excluded the last two examinations of AFP before the detection of HCC. The results of the analysis also showed average integration value of AFP as a significant predictive factor for incidence of HCC.

Male gender was also identified as an independent risk factor for HCC in non-SVR patients in this study. Several reports have shown that men are at a higher risk of developing HCC than women [6, 10, 33, 40, 41]. The male gender also appears to be a risk factor for more severe disease and a greater risk of developing cirrhosis in chronic hepatitis C [42]. Although the association of male gender with the risk of HCC is as yet unexplained, hormonal or genetic factors may lead to increased risk for HCC and cirrhosis in men as previously discussed [10].

In conclusion, a decrease in the AFP integration value predicts reduced incidence of HCC in patients with hepatitis C receiving interferon therapy. Further prospective studies with a larger number of patients are required to validate the significance of these findings.

Acknowledgments This work was supported by Grants-in-aid for Scientific Research from the Ministry of Education, Culture, Sports, Science and Technology, and the Ministry of Health, Labor and Welfare of Japan.

Conflict of interest The authors declare that they have no conflict of interest.

References

1. Bruix J, Barrera JM, Calvet X, Ercilla G, Costa J, Sanchez-Tapias JM, Ventura M, Vall M, Bruguera M, Bru C, et al. Prevalence of antibodies to hepatitis C virus in Spanish patients with hepatocellular carcinoma and hepatic cirrhosis. Lancet. 1989;2:1004–6.
2. Colombo M, Kuo G, Choo QL, Donato MF, Del Ninno E, Tommasini MA, Dioguardi N, Houghton M. Prevalence of antibodies to hepatitis C virus in Italian patients with hepatocellular carcinoma. Lancet. 1989;2:1006–8.
3. Hasan F, Jeffers LJ, De Medina M, Reddy KR, Parker T, Schiff ER, Houghton M, Choo QL, Kuo G. Hepatitis C-associated hepatocellular carcinoma. Hepatology. 1990;12:589–91.
4. Ikeda K, Saitoh S, Koida I, Arase Y, Tsubota A, Chayama K, Kumada H, Kawanishi M. A multivariate analysis of risk factors for hepatocellular carcinogenesis: a prospective observation of 795 patients with viral and alcoholic cirrhosis. Hepatology. 1993;18:47–53.
5. Tsukuma H, Hiyama T, Tanaka S, Nakao M, Yabuuchi T, Kitamura T, Nakanishi K, Fujimoto I, Inoue A, Yamazaki H, et al. Risk factors for hepatocellular carcinoma among patients with chronic liver disease. N Engl J Med. 1993;328:1797–801.
6. Fattovich G, Stroffolini T, Zagni I, Donato F. Hepatocellular carcinoma in cirrhosis: incidence and risk factors. Gastroenterology. 2004;127:S35–50.
7. Ikeda K, Marusawa H, Osaki Y, Nakamura T, Kitajima N, Yamashita Y, Kudo M, Sato T, Chiba T. Antibody to hepatitis B core antigen and risk for hepatitis C-related hepatocellular carcinoma: a prospective study. Ann Intern Med. 2007;146:649–56.
8. Liang TJ, Heller T. Pathogenesis of hepatitis C-associated hepatocellular carcinoma. Gastroenterology. 2004;127:S62–71.
9. Yoshida H, Shiratori Y, Moriyama M, Arakawa Y, Ide T, Sata M, Inoue O, Yano M, Tanaka M, Fujiyama S, Nishiguchi S, Kuroki T, Imazeki F, Yokosuka O, Kinoyama S, Yamada G, Omata M. Interferon therapy reduces the risk for hepatocellular carcinoma: national surveillance program of cirrhotic and noncirrhotic patients with chronic hepatitis C in Japan. IHIT Study Group. Inhibition of hepatocarcinogenesis by interferon therapy. Ann Intern Med. 1999;131:174–81.
10. Heathcote EJ. Prevention of hepatitis C virus-related hepatocellular carcinoma. Gastroenterology. 2004;127:S294–302.
11. Lok AS, Seeff LB, Morgan TR, di Bisceglie AM, Sterling RK, Curto TM, Everson GT, Lindsay KL, Lee WM, Bonkovsky HL, Dienstag JL, Ghany MG, Morishima C, Goodman ZD. Incidence of hepatocellular carcinoma and associated risk factors in hepatitis C-related advanced liver disease. Gastroenterology. 2009; 136:138–48.
12. Effect of interferon-alpha on progression of cirrhosis to hepatocellular carcinoma: a retrospective cohort study. International Interferon-alpha Hepatocellular Carcinoma Study Group. Lancet. 1998;351:1535–9.
13. Camma C, Giunta M, Andreone P, Craxi A. Interferon and prevention of hepatocellular carcinoma in viral cirrhosis: an evidence-based approach. J Hepatol. 2001;34:593–602.
14. Di Bisceglie AM, Shiffman ML, Everson GT, Lindsay KL, Everhart JE, Wright EC, Lee WM, Lok AS, Bonkovsky HL, Morgan TR, Ghany MG, Morishima C, Snow KK, Dienstag JL. Prolonged therapy of advanced chronic hepatitis C with low-dose peginterferon. N Engl J Med. 2008;359:2429–41.
15. Fattovich G, Giustina G, Degos F, Diodati G, Tremolada F, Nevens F, Almasio P, Solinas A, Brouwer JT, Thomas H, Realdi G, Corrocher R, Schalm SW. Effectiveness of interferon alfa on incidence of hepatocellular carcinoma, decompensation in cirrhosis type C. European Concerted Action on Viral Hepatitis (EUROHEP). J Hepatol. 1997;27:201–5.
16. Hayashi K, Kumada T, Nakano S, Takeda I, Kiriyama S, Sone Y, Toyoda H, Shimizu H, Honda T. Incidence of hepatocellular carcinoma in chronic hepatitis C after interferon therapy. Hepatogastroenterology. 2002;49:508–12.
17. Lok AS, Everhart JE, Wright EC, Di Bisceglie AM, Kim HY, Sterling RK, Everson GT, Lindsay KL, Lee WM, Bonkovsky HL, Dienstag JL, Ghany MG, Morishima C, Morgan TR. Maintenance peginterferon therapy and other factors associated with hepatocellular carcinoma in patients with advanced hepatitis C. Gastroenterology. 2011;140:840–9.
18. Nishiguchi S, Kuroki T, Nakatani S, Morimoto H, Takeda T, Nakajima S, Shiomi S, Seki S, Kobayashi K, Otani S. Randomised trial of effects of interferon-alpha on incidence of hepatocellular carcinoma in chronic active hepatitis C with cirrhosis. Lancet. 1995;346:1051–5.
19. Okanoue T, Itoh Y, Minami M, Sakamoto S, Yasui K, Sakamoto M, Nishioji K, Murakami Y, Kashima K. Interferon therapy lowers the rate of progression to hepatocellular carcinoma in chronic hepatitis C but not significantly in an advanced stage: a retrospective study in 1148 patients. Viral Hepatitis Therapy Study Group. J Hepatol. 1999;30:653–9.
20. Izuno K, Fujiyama S, Yamasaki K, Sato M, Sato T. Early detection of hepatocellular carcinoma associated with cirrhosis by combined assay of des-gamma-carboxy prothrombin and alpha-fetoprotein: a prospective study. Hepatogastroenterology. 1995;42:387–93.

21. Trevisani F, D'Intino PE, Morselli-Labate AM, Mazzella G, Accogli E, Caraceni P, Domenicali M, De Notariis S, Roda E, Bernardi M. Serum alpha-fetoprotein for diagnosis of hepatocellular carcinoma in patients with chronic liver disease: influence of HBsAg and anti-HCV status. J Hepatol. 2001;34:570–5.
22. Zoli M, Magalotti D, Bianchi G, Gueli C, Marchesini G, Pisi E. Efficacy of a surveillance program for early detection of hepatocellular carcinoma. Cancer. 1996;78:977–85.
23. Alpert E, Feller ER. Alpha-fetoprotein (AFP) in benign liver disease. Evidence that normal liver regeneration does not induce AFP synthesis. Gastroenterology. 1978;74:856–8.
24. Bloomer JR, Waldmann TA, McIntire KR, Klatskin G. Alpha-fetoprotein in noneoplastic hepatic disorders. JAMA. 1975;233:38–41.
25. Ruoslahti E, Seppala M. Normal and increased alpha-fetoprotein in neoplastic and non-neoplastic liver disease. Lancet. 1972;2:278–9.
26. Sakurai T, Marusawa H, Satomura S, Nabeshima M, Uemoto S, Tanaka K, Chiba T. *Lens culinaris* agglutinin-A-reactive alpha-fetoprotein as a marker for liver atrophy in fulminant hepatic failure. Hepatol Res. 2003;26:98–105.
27. Taketa K. Alpha-fetoprotein: reevaluation in hepatology. Hepatology. 1990;12:1420–32.
28. Di Bisceglie AM, Sterling RK, Chung RT, Everhart JE, Dienstag JL, Bonkovsky HL, Wright EC, Everson GT, Lindsay KL, Lok AS, Lee WM, Morgan TR, Ghany MG, Gretch DR. Serum alpha-fetoprotein levels in patients with advanced hepatitis C: results from the HALT-C Trial. J Hepatol. 2005;43:434–41.
29. Tateyama M, Yatsuhashi H, Taura N, Motoyoshi Y, Nagaoka S, Yanagi K, Abiru S, Yano K, Komori A, Migita K, Nakamura M, Nagahama H, Sasaki Y, Miyakawa Y, Ishibashi H. Alpha-fetoprotein above normal levels as a risk factor for the development of hepatocellular carcinoma in patients infected with hepatitis C virus. J Gastroenterol. 2011;46:92–100.
30. Murashima S, Tanaka M, Haramaki M, Yutani S, Nakashima Y, Harada K, Ide T, Kumashiro R, Sata M. A decrease in AFP level related to administration of interferon in patients with chronic hepatitis C and a high level of AFP. Dig Dis Sci. 2006;51:808–12.
31. Tamura Y, Yamagiwa S, Aoki Y, Kurita S, Suda T, Ohkoshi S, Nomoto M, Aoyagi Y. Serum alpha-fetoprotein levels during and after interferon therapy and the development of hepatocellular carcinoma in patients with chronic hepatitis C. Dig Dis Sci. 2009;54:2530–7.
32. Arase Y, Ikeda K, Suzuki F, Suzuki Y, Kobayashi M, Akuta N, Hosaka T, Sezaki H, Yatsuji H, Kawamura Y, Kumada H. Prolonged-interferon therapy reduces hepatocarcinogenesis in aged-patients with chronic hepatitis C. J Med Virol. 2007;79:1095–102.
33. Asahina Y, Tsuchiya K, Tamaki N, Hirayama I, Tanaka T, Sato M, Yasui Y, Hosokawa T, Ueda K, Kuzuya T, Nakanishi H, Itakura J, Takahashi Y, Kurosaki M, Enomoto N, Izumi N. Effect of aging on risk for hepatocellular carcinoma in chronic hepatitis C virus infection. Hepatology. 2010;52:518–27.
34. Ohno O, Mizokami M, Wu RR, Saleh MG, Ohba K, Orito E, Mukaide M, Williams R, Lau JY. New hepatitis C virus (HCV) genotyping system that allows for identification of HCV genotypes 1a, 1b, 2a, 2b, 3a, 3b, 4, 5a, and 6a. J Clin Microbiol. 1997;35:201–7.
35. Kumada T, Toyoda H, Kiriyama S, Sone Y, Tanikawa M, Hisanaga Y, Kanamori A, Atsumi H, Takagi M, Nakano S, Arakawa T, Fujimori M. Incidence of hepatocellular carcinoma in hepatitis C carriers with normal alanine aminotransferase levels. J Hepatol. 2009;50:729–35.
36. Arase Y, Ikeda K, Suzuki F, Suzuki Y, Kobayashi M, Akuta N, Hosaka T, Sezaki H, Yatsuji H, Kawamura Y, Kumada H. Interferon-induced prolonged biochemical response reduces hepatocarcinogenesis in hepatitis C virus infection. J Med Virol. 2007;79:1485–90.
37. Kasahara A, Hayashi N, Mochizuki K, Takayanagi M, Yoshioka K, Kakumu S, Iijima A, Urushihara A, Kiyosawa K, Okuda M, Hino K, Okita K. Risk factors for hepatocellular carcinoma, its incidence after interferon treatment in patients with chronic hepatitis C. Osaka Liver Disease Study Group. Hepatology. 1998;27:1394–402.
38. Kurokawa M, Hiramatsu N, Oze T, Mochizuki K, Yakushijin T, Kurashige N, Inoue Y, Igura T, Imanaka K, Yamada A, Oshita M, Hagiwara H, Mita E, Ito T, Inui Y, Hijioka T, Yoshihara H, Inoue A, Imai Y, Kato M, Kiso S, Kanto T, Takehara T, Kasahara A, Hayashi N. Effect of interferon alpha-2b plus ribavirin therapy on incidence of hepatocellular carcinoma in patients with chronic hepatitis. Hepatol Res. 2009;39:432–8.
39. Suzuki K, Ohkoshi S, Yano M, Ichida T, Takimoto M, Naitoh A, Mori S, Hata K, Igarashi K, Hara H, Ohta H, Soga K, Watanabe T, Kamimura T, Aoyagi Y. Sustained biochemical remission after interferon treatment may closely be related to the end of treatment biochemical response and associated with a lower incidence of hepatocarcinogenesis. Liver Int. 2003;23:143–7.
40. Kurosaki M, Hosokawa T, Matsunaga K, Hirayama I, Tanaka T, Sato M, Yasui Y, Tamaki N, Ueda K, Tsuchiya K, Kuzuya T, Nakanishi H, Itakura J, Takahashi Y, Asahina Y, Enomoto N, Izumi N. Hepatic steatosis in chronic hepatitis C is a significant risk factor for developing hepatocellular carcinoma independent of age, sex, obesity, fibrosis stage and response to interferon therapy. Hepatol Res. 2010;40:870–7.
41. Takahashi H, Mizuta T, Eguchi Y, Kawaguchi Y, Kuwashiro T, Oeda S, Isoda H, Oza N, Iwane S, Izumi K, Anzai K, Ozaki I, Fujimoto K. Post-challenge hyperglycemia is a significant risk factor for the development of hepatocellular carcinoma in patients with chronic hepatitis C. J Gastroenterol. 2011;46:790–8.
42. Forns X, Ampurdanes S, Sanchez-Tapias JM, Guilera M, Sans M, Sanchez-Fueyo A, Quinto L, Joya P, Bruguera M, Rodes J. Long-term follow-up of chronic hepatitis C in patients diagnosed at a tertiary-care center. J Hepatol. 2001;35:265–71.

Hepatology Research 2012; 42: 999–1007 doi: 10.1111/j.1872-034X.2012.01019.x

Original Article

Visualization of blood drainage area from hypervascular hepatocellular carcinoma on ultrasonographic images during hepatic arteriogram: Comparison with depiction of drainage area on contrast-enhanced ultrasound

Ryuichi Kita,[1] Azusa Sakamoto,[1] Yoshiaki Nagata,[4] Norihiro Nishijima,[5] Atsuyuki Ikeda,[5] Hiroo Matsuo,[1] Mitsumasa Okada,[2] Shinji Ashida,[2] Toshikatsu Taniguchi,[3] Toru Kimura[1] and Yukio Osaki[1]

Departments of [1]Gastroenterology and Hepatology, [2]Angiography and [3]Ultrasonographics, Osaka Red Cross Hospital, [4]Department of Gastroenterology and Hepatology, Kinki University School of Medicine, Osaka, and [5]Department of Gastroenterology and Hepatology, Kyoto University Graduate School of Medicine, Kyoto, Japan

Aim: Corona enhancement is the visualized drainage area from a hypervascular tumor observed on single-level dynamic computed tomography during hepatic arteriography (CTHA) and is thought to be a high-risk area for micrometastases. However, because it cannot be visualized with ordinary ultrasonography (US), we aimed to visualize corona enhancement on US by means of arterial injection of the contrast material and to measure its thickness.

Method: Forty-one hypervascular hepatocellular carcinoma (HCC) cases were prospectively investigated. US during hepatic arteriography (USHA) was executed by means of selective injection of the contrast material perfluorobutane (Sonazoid) from the hepatic artery. Ordinary contrast-enhanced US with venous administration of contrast material and single-level dynamic CTHA were also performed.

Results: Corona enhancement was observed in 36 cases (88%) on USHA and in 25 cases (61%) on single-level dynamic CTHA. The thickness of corona enhancement of 36 cases visualized with USHA ranged 3.1–18.4 mm and the mean thickness ± standard deviation was 6.0 ± 3.0 mm. Thickness of corona enhancement was less than 10.0 mm in 34 cases (94%).

Conclusion: Corona enhancement could be visualized even on US images, and the average thickness of them was 6 mm.

Key words: ablative margin, corona enhancement, single-level dynamic computed tomography during hepatic arteriography, Sonazoid, ultrasonography during hepatic arteriography

INTRODUCTION

HEPATOCELLULAR CARCINOMA (HCC) is one of the most common worldwide malignancies and has been treated aggressively with surgery, local ablation and transcatheter intervention therapies in Japan. Diagnostic modalities such as ultrasonography (US), dynamic contrast study of computed tomography (CT) and magnetic resonance imaging (MRI) have been employed for imaging diagnosis of the hepatic nodules. Especially, CT during hepatic arteriography (CTHA) and CT during arterial portography (CTAP) are two of the most accurate modalities for evaluating arterial and portal venous flow in hepatic nodules.[1–3] Moreover, single-level dynamic CTHA studies, the protocol of continuous observation of a given slice on CTHA, have yielded outstanding data about drainage flow from hypervascular nodules.[4–10] In short, this flow can be visualized as a ring-like enhanced area, known as corona enhancement, around the nodules in late-phase single-level dynamic CTHA studies. It has been reported, based on knowledge of resected tumors and recurrence patterns, that local recurrence of HCC frequently occurs in

Correspondence: Dr Ryuichi Kita, Department of Gastroenterology and Hepatology, Osaka Red Cross Hospital; 5-53 Fudegasaki-cho, Tennoji-ku, Osaka 543-8555, Japan. Email: r-kita@osaka-med.jrc.or.jp
Received 21 April 2011; revision 16 December 2011; accepted 27 March 2012.

the corona enhancement area.[11] This might lead to the recommendation that resection or ablation of tumors should include corona enhancement areas.

In January 2007, a new contrast agent for US imaging was released in Japan. Sonazoid (Daiichi Sankyo, Tokyo, Japan) is a lipid-stabilized suspension of perfluorobutane microbubbles and it can visualize enhanced images without destroying the contrast material, which enables a continuous observation of the target organs and vascularities.[12,13] Recently, local ablation therapies such as radio frequency ablation (RFA), which rely on depiction by US, are employed frequently for the treatment of HCC. However, corona enhancement cannot be visualized by contrast-enhanced US with ordinary administration of contrast material from the cubital vein. To depict corona enhancement on US, we used selective arterial injection of contrast material Sonazoid from the hepatic artery and observed the inflow to and outflow from the nodule. The invasiveness of US during intra-arterial contrast injection was similar to that of CT during hepatic arteriography. The primary purpose of this angiographic procedure was interventional therapy, and our study was planned on the opportunities of primary schedules of interventional angiographic procedure. Moreover, we compared the corona enhancement pictures obtained with this method with those on ordinary contrast-enhanced US depiction with venous administration of contrast material. The main purpose of this study was to verify the visualization of corona enhancement in US images.

METHODS

THE VARIOUS PROTOCOLS and consent forms of the study were approved by the Ethics Committee of Osaka Red Cross Hospital and written informed consent was obtained from each patient.

Tumors

Abdominal angiography was administrated to 794 patients between September 2007 and September 2008 at the Osaka Red Cross Hospital for further examination or angiographic intervention therapy for liver diseases. At the Osaka Red Cross Hospital, an average of 16 cases are subjected to abdominal angiography per week, and a large majority of these cases are HCC. Because of limited time available in view of clinical duties, only one HCC case per week was selected for this study. Of the 45 patients who consented to undergo US during hepatic angiography, 41 hypervascular HCC clearly depicted on non-contrasted US were selected to be analyzed for this study. No cases with HCC identified near the portal venous vein were included.

Diagnosis of HCC had been made based on findings obtained with imaging and serological examinations: hypervascularity in the arterial phase and washout image in the portal phase in the hemodynamic study, and elevation of serum levels of hepatic tumor markers (α-fetoprotein [AFP] >400 ng/mL and/or des-γ-carboxy prothrombin [DCP] >100 mIU/mL). All 11 cases with newly developed tumors less than 20 mm in diameter had been previously diagnosed and treated as hypervascular HCC, and these tumors were thought to constitute recurrences of known HCC. If neither AFP nor DCP showed the above-mentioned elevations in cases with tumors more than or equal to 20 mm in diameter, histological examinations were performed. Aspiration biopsies were carried out in nine cases including the ones mentioned above, and all of them were diagnosed as HCC.

As for the background liver disease, 31 cases were clinically diagnosed as cirrhosis and 10 as chronic hepatitis. HBs antigen was positive in five cases and hepatitis C virus antibody in 27 cases. One case showed positivity for anti-mitochondrial antibody and was diagnosed as primary biliary cirrhosis. Tumors were single nodules in 29 cases and multiple in the rest, and their size ranged 13–49 mm in diameter with a mean ± standard deviation of 27 ± 15 mm. The tumor diameter was less than 20 mm in 12 cases, equal to or more than 20 mm and less than 30 mm in 15 cases, and equal to or more than 30 mm in 14 cases.

After imaging with intra-arterial injection including US during hepatic arteriography (USHA), transarterial chemoembolization was applied to 31 cases. RFA was performed for 17 cases and hepatic resections for complete curability for 10 cases.

CT during angiography

A unified helical CT and angiography system (INFX-8000C, IVR-CT/Angiography system; Toshiba Medical Systems, Tokyo, Japan) was employed for digital subtraction angiography and CT during intra-arterial injection of contrast material. This system consists of an angiography unit and a CT unit arranged in a linear configuration, which facilitates safe and rapid transfer of the patient from one unit to the other.

Computed tomography during hepatic arteriography was performed as follows. A catheter tip was placed in the common or proper hepatic artery under fluoroscopic guidance with help of injections of X-ray contrast agents. Fifteen to thirty milliliters of 150 mgI/mL

of contrast material (350 mgI/mL, Imagenil; Guerbet Japan, Tokyo, Japan) diluted with saline was injected at 1.2–2.5 mL/s with reference to the patient's physique and rough estimate of blood flow. CT scan was started 5 s after the start of contrast material injection. CT was performed with a table speed of 9.3 mm/s, 7-mm beam collimation and image reconstruction of 7 mm-thick sections. Tube voltage and current were 120 kV and 150 mAs, respectively.

Single-level dynamic CTHA was performed in all cases after CTHA. The appropriate craniocaudal level for this procedure was determined on the basis of CTHA images of the tumor. Single-level dynamic CTHA was performed with the infusion of 150 mgI/mL contrast material at the same rate as for CTHA for 6 s from the same arterial position. The CT scan was started at an appropriate set level immediately after the start of contrast material injection with 5-mm beam collimation and image reconstruction of 5 mm-thick sections. Thirty-second continuous scanning without table feed was performed during a single breath hold, and the images were reconstructed at 1-s intervals. During the procedure, oxygen was administrated at a rate of 2 L/min to help the patients cope with the long breath hold.

USHA

For ultrasonographic depiction, we used the Aplio 50 (Toshiba Medical Systems Inc., Tokyo, Japan) in the coded harmonic imaging (CHI)-low mode. The mechanical index was adjusted between 0.2 and 0.3, the focus was on the deepest level of the nodule and the frame rate was 15 frames/s. Sonazoid was dissolved according to the manufacturer's instructions and the solution was diluted with saline to 1:100 just before use for USHA. Four milliliters of a final concentration of 0.08 mL/mL of perfluorobutane solution was injected from the common or proper hepatic artery at 1 mL/s for 4 s to observe the enhancement of nodule and surrounding parenchyma. Concentration and volume of Sonazoid injected were calculated and decided in accordance with the dose used for i.v. administration of Sonazoid and the ratio of iodine contrast materials used for i.v. dynamic CT and single-level dynamic CTHA at our institution.

Contrast-enhanced US

For contrast-enhanced US, we also used Aplio 50 in the CHI-low mode. The mechanical index, focus and frame rate were the same as those of USHA. Sonazoid was dissolved according to the manufacturer's instructions and 0.5 mL of the solution was injected from the cubital vein for approximately 1 s. Five milliliters of saline was injected to push out residual Sonazoid in the injection route immediately after Sonazoid injection.

Analysis

Ultrasonography and CT images were analyzed after the still and motion pictures had been obtained with the various procedures. After injection of contrast material, the tumor was enhanced, after which the contrast material was washed out. A ring-like enhancement in surrounding parenchyma was then observed as a drainage area when single-level dynamic CTHA was used, and this phenomenon was called a corona enhancement.[4] The same image could be observed with USHA, which we also defined as corona enhancement for this method. Thickness of corona enhancement was measured by one individual (K. R.) using software supplied with the US equipment (Aplio 50; Toshiba Medical Systems) for measurement on USHA. Measurement of corona thickness was based on the most clearly depicted images obtained 16–20 s after arterial injection of Sonazoid. Because the thickness of corona enhancement can differ even in one HCC, the greatest thickness was adopted as the corona thickness.

We also measured the diameters of tumor images before and after contrast enhancement during contrast-enhanced US together with i.v. administration of Sonazoid. We then calculated the difference between these two diameters by subtraction, and divided them by 2 to obtain the average increase in length on either side. These lengths were compared with corona thickness measured with USHA.

Radiofrequency ablation was performed in 17 cases, all of which had been treated with transcatheter chemoembolization before RFA. Therefore, we analyzed the relationship between the size of the ablative margins in relation to corona thickness and local recurrences.

Statistical analysis

Statistical analysis was performed using SPSS ver. 18.0.0 (SPSS , Chicago, IL, USA). Mean and standard deviation of the mean (SD) were calculated by the usual method. All values are expressed as means ± SD. The Kruskal–Wallis H test was used for a comparative evaluation of the parameters affecting thickness of corona enhancement. $P < 0.05$ was considered statistically significant.

RESULTS

NO ADVERSE EVENTS occurred during the sequential angiographic study using either USHA or CTHA. Among the total of 41 hypervascular HCC,

corona enhancement was observed in 36 cases (88%) on USHA, in 25 cases (61%) on single-level dynamic CTHA and in 24 cases (59%) on both (Figs 1–3), but could not be detected on either USHA or single-level dynamic CTHA in four cases (10%). None of the cases showed corona enhancement on ordinary contrast-enhanced US images with venous injection of the contrast material.

The thickness of corona enhancement ranged 3.1–18.4 mm with a mean thickness ± SD of 6.0 ± 3.0 mm on USHA of 36 cases (Table 1).

Corona enhancement less than 10.0 mm in thickness was observed on USHA of 34 cases (94%). In relation to the tumor size, thickness of corona enhancement was 4.3 ± 1.3 mm for tumors less than 2 cm in diameter, 6.4 ± 2.6 mm for tumors 2 cm to less than 3 cm in diameter and 7.2 ± 3.8 mm for tumors of 3 cm or more in diameter (Fig. 4, Table 2). A statistically significant correlation was found between the tumor size and the thickness of corona enhancement (Kruskal–Wallis H test, $P < 0.01$).

For the 26 cases evaluated, the thickness of expanded enhanced area measured by contrast-enhanced US were 4.1 ± 2.6 mm and correlated well with corona width measured with USHA (Pearson's correlation coefficient: $r = 0.74$).

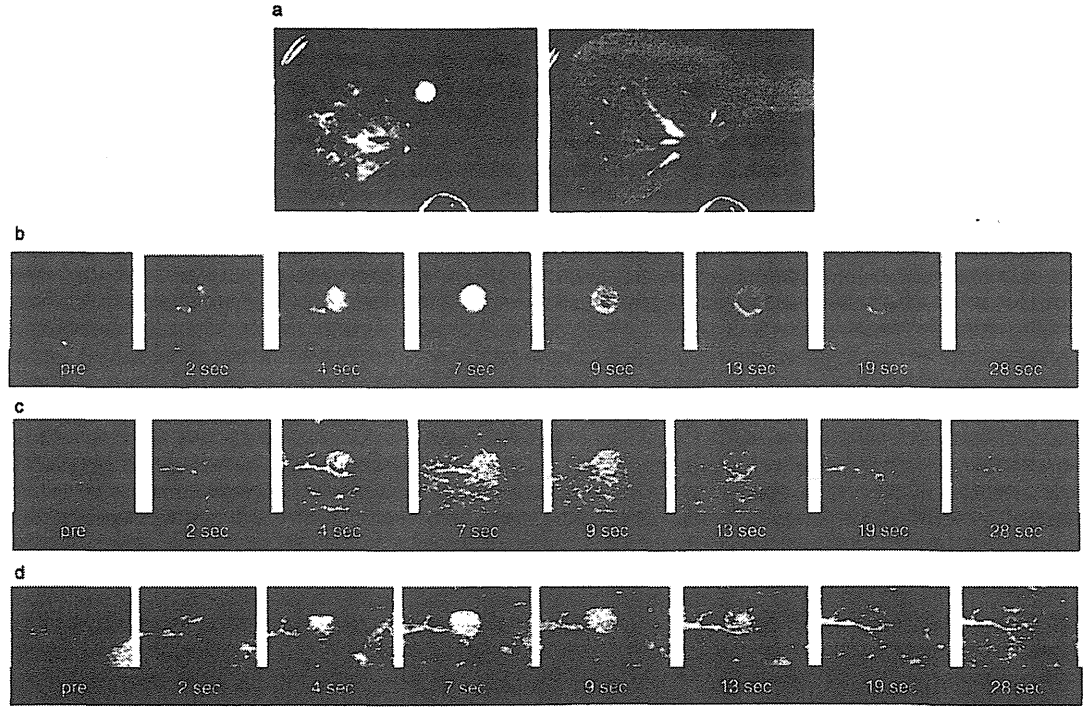

Figure 1 A 69-year-old female with recurrence of HCC 1.5 cm in diameter in segment 2. (a) CTHA (left) and CTAP images. Tumor was enhanced on CTHA and showed a flawed image on CTAP. (b) Images of the tumor on single-level dynamic CTHA, which was performed just before and 2, 4, 7, 9, 13, 19 and 28 s after injection of contrast material from the common hepatic artery. (c) Images of the tumor on USHA at the same times before and after injection of contrast material in the same manner as for CTHA. (d) Images of the tumor on ordinary contrasted US obtained at the same times as for CTHA and USHA after the beginning of the enhancement procedure. (b–d) Slightly larger area became enhanced in 7–13 s after the start of enhancement. Enhancement of the real tumor area became faint and corona enhancement became visible as seen in (b) and (c) but not in (d). CTAP, computed tomography during arterial portography; CTHA, computed tomography during hepatic arteriography; HCC, hepatocellular carcinoma; USHA ultrasonography during hepatic arteriography.

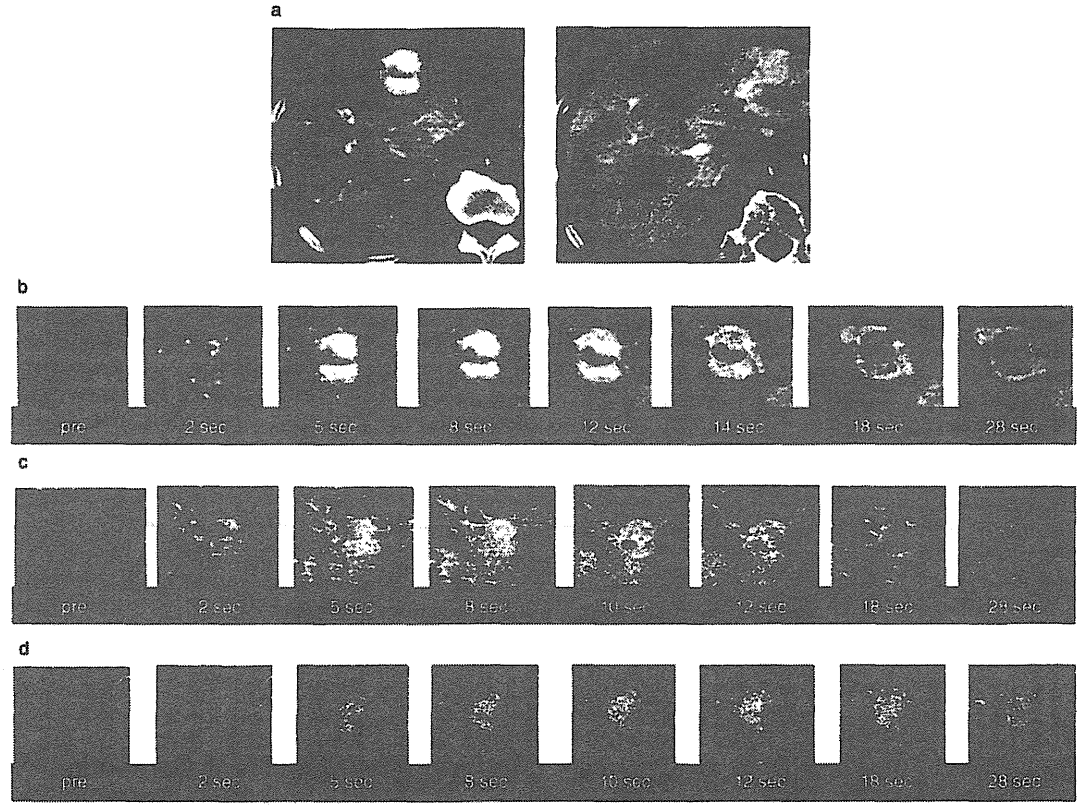

Figure 2 A 77-year-old male with HCC 3.3 cm in diameter in segment 4. (a) Images of CTHA (left) and CTAP. Multiple liver cysts are also shown. The hypervascular tumor in segment 4 was enhanced on CTHA and showed a flawed image on CTAP. The poorly enhanced part of the tumor is depicted on CTHA in this slice while the resection specimen showed that this region corresponded to a rather well-differentiated carcinoma (data not shown). (b–d) Serial images of single-level dynamic CTHA, USHA and ordinary contrast-enhanced US. (b) Images obtained with single-level dynamic CTHA just before and 2, 5, 8, 12, 14, 18 and 28 s after injection of contrast material. The tumor itself was enhanced in 8 s and a slightly wider area around the tumor became enhanced after that. Enhancement of the inner part corresponding to the tumor itself became faint and corona enhancement became visible in 18 s. (c) Images obtained with USHA just before and 2, 5, 8, 10, 12, 18 and 28 s after injection of contrast material. (d) Images obtained with ordinary contrasted US at the same times as for USHA. A slightly larger area became enhanced in (c) and (d) 10 s after the start of enhancement. Enhancement of the real tumor area became faint and the contour of the tumor became visible as corona enhancement in (c) but not in (d). The differences in enhanced areas and shapes between CTHA and USHA could be accounted for by differences in cross-section between CT and US. CT, computed tomography; CTAP, computed tomography during arterial portography; CTHA, computed tomography during hepatic arteriography; HCC, hepatocellular carcinoma; RFA, radio frequency ablation; US, ultrasonography; USHA ultrasonography during hepatic arteriography.

Ablative margins evaluated after the procedure were larger than the measured corona thickness in five cases and smaller in 12. Local recurrence occurring within 1 year could be evaluated in five and 11 cases, and within 2 years in two and 10 cases, respectively, and local recurrence was detected in zero and three cases within 1 year and in zero and six cases within 2 years, respectively.

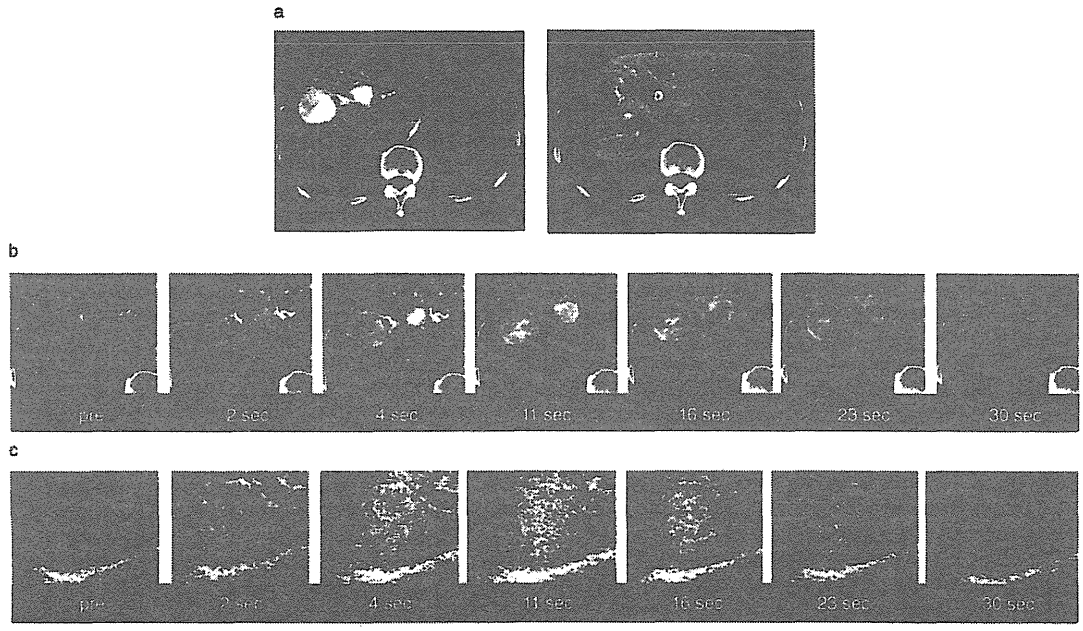

Figure 3 A 71-year-old male with HCC 4.2 cm in diameter in segment 8. (a) Images of CTHA (left) and CTAP. Tumor was enhanced on CTHA and showed a flawed image on CTAP. Hypervascular tumor in segment 4 is also depicted. (b) Images of the tumor on single-level dynamic CTHA, which was performed just before and 2, 4, 11, 16, 23 and 30 s after injection of contrast material from the appropriate hepatic artery. (c) Images of the tumor on US during hepatic arteriography taken at the same times before and after injection of contrast material from the same place. A slightly larger area became enhanced in (c) 11 s after the start of enhancement. Enhancement of the real tumor area became faint and corona enhancement became visible. Images of ordinary contrast-enhanced US are not shown here because they were not obtained serially with the same dimensions. CTAP, computed tomography during arterial portography; CTHA, computed tomography during hepatic arteriography; HCC, hepatocellular carcinoma; US, ultrasonography.

DISCUSSION

RECENTLY, RFA HAS become one of the most commonly used options for treating HCC in Japan. But as the number of cases treated with RFA has increased, sometimes local recurrences adjoining the ablated area have been observed, which might be avoided by making the ablated area wider. Some investigators reported that a satisfactory ablative margin around the tumor is necessary for suppressing local recurrence.[14–17] Nakazawa *et al.* concluded from their analysis of clinical data for the cumulative rate of local tumor progression at 3 years that an ablative margin of less than 5 mm was a significant independent risk factor for local tumor progression.[15] Nishijima *et al.* also showed that the cumulative rate of local tumor recurrence had gradually worsened in proportion to the lack of an ablative margin of at least 5 mm from the tumor edge.[17] Moreover, Sakon *et al.* observed that local recurrence frequently occurred in the corona enhancement area surrounding the tumor, which corresponds to the drainage area of the hypervas-

Table 1 Thickness of corona enhancement area measured on USHA

Cases	36
Minimum	3.1 mm
Maximum	18.4 mm
Average ± SD	6.0 ± 3.0 mm
Median	5.3 mm
Cases with <10 mm of corona thickness	34 cases (94%)

SD, standard deviation; USHA, ultrasonography during hepatic arteriography.

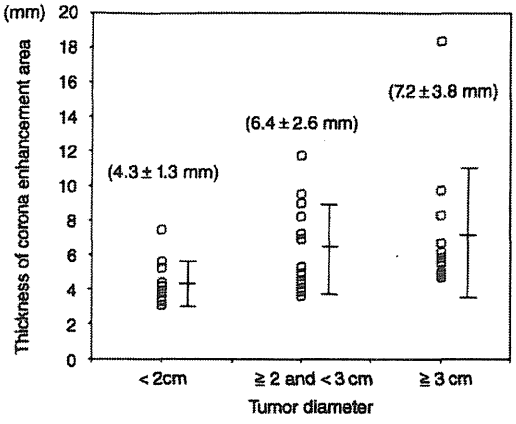

Figure 4 Distribution of thickness of corona enhancement area measured on USHA in relation to tumor diameter. A statistically significant correlation was found between the tumor size and the thickness of corona enhancement (Kruskal–Wallis H test, $P < 0.01$). USHA, ultrasonography during hepatic arteriography.

cular tumor.[11] On their observations of resected tumors and recurrence patterns, they recommended that resection or ablation of tumors should include the corona enhancement areas. These reported findings, both pathological and clinical, indicate the frequent presence of tumor cells in the corona enhancement area.

Because the procedure of RFA is almost always carried out while being monitored on US, detection of the recommended ablative margin on US is highly desirable. However, corona enhancement cannot be visualized with ordinary contrast-enhanced US under venous administration of contrast material from the medial cubital vein, which has resulted in poor definition of the required ablative margin on US imaging. The poor depiction of corona enhancement on ordinary US images is likely to be mainly caused by the delayed and extended enhancement time followed by portal inflow with a slight time lag. Because single-level dynamic CTHA can produce a sharp image of corona enhancement by selective arterial injection of contrast material, similar pictures must be obtained in the same manner by selective arterial injection of limited contrast material in a short period.

In our study, we could depict corona enhancement in 88% of hypervascular HCC on USHA. A smaller ablative margin is likely to increase the risk of local recurrence, while an ablative margin that is too wide could cause unnecessary liver damage. So, most physicians doing RFA in Japan have intended to create ablative margins of more than 5 mm according to aforementioned reports. To estimate the appropriate ablative margins, we measured the thickness of corona enhancement on USHA. The thickness of corona enhancement ranged 3.1–18.4 mm and their mean thickness was 6.0 mm. Cases with corona enhancement less than 10.0 mm in thickness accounted for 94% of enhancement observed on USHA. These findings appear to be consistent with those for recurrence and ablative margin on RFA reported by Nakazawa *et al.* and Nishijima *et al.* namely, that the absence of an ablative margin of at least 5 mm significantly correlated with local tumor progression.[15,17] This also accounts for the distribution of small satellite lesions detected histologically by Nakashima *et al.*[18] Moreover, examination of the relationship between the thickness of corona enhancement and tumor size revealed that corona enhancement became thicker as the tumor size increased (Fig. 4, Table 2), which leads us to recommend using ablative margins related to tumor size whenever possible.

Table 2 Thickness of corona enhancement area measured on USHA in relation to tumor diameter

	Diameter of the tumor		
	<2 cm	≥2 and <3 cm	≥3 cm
Cases	11	13	12
Minimum	3.1 mm	3.6 mm	4.7 mm
Maximum	7.4 mm	11.7 mm	18.4 mm
Average ± SD	4.3 ± 1.3 mm	6.4 ± 2.6 mm	7.2 ± 3.8 mm
Median	3.8 mm	5.3 mm	5.8 mm
Cases with <10 mm of corona thickness	11 cases (100%)	12 cases (92%)	11 cases (92%)

A statistically significant correlation was found between the tumor size and the thickness of corona enhancement (Kruskal–Wallis H test, $P < 0.01$)
SD, standard deviation; USHA, ultrasonography during hepatic arteriography.

To evaluate the significance of ablation including corona enhancement area, we analyzed the relationship between the size of the ablative margins in relation to corona thickness and local recurrences. No local recurrences occurred in cases where ablative margins evaluated after the procedure were larger than the measured corona thickness. Although the number of cases was small, we could also show that an ablative margin larger than the measured corona thickness may be necessary for the avoidance of local recurrences in ablative therapy.

We could also demonstrate by comparison of USHA and ordinary contrast-enhanced US that corona enhancement was depicted with the latter technique included in the edge of the enhanced area without boundary between corona and tumor enhancement. The thickness of these expanded area measured by contrast-enhanced US were on average 2 mm thinner than corona widths measured by USHA. There are two possible reasons to account for the difference between these measurements. The first is that corona widths measured by USHA may include stains remaining from the capsule or the inner edge of the tumor. The second is that the diameter measured on pre-contrast US images may include some non-tumoral parenchyma in the periphery, for example, a dilated sinusoid.

We could confirm the existence of corona enhancement on either USHA or single-level dynamic CTHA in 37 out of 41 (90%) hypervascular HCC cases. Failure to detect corona enhancement might be caused by inaccuracy of breath holding during examination, which drove tumor images out of observation range. Two-phase CTHA is currently widely used, but our study was done in 2007 and 2008 when only single-level dynamic CTHA was available. This might make the detection of corona enhancement on CT during angiography incomplete. In comparison to single-level dynamic CTHA, USHA might achieve a superior detection rate of corona enhancement due to manual adjustment of depicting image section.

First-generation i.v. US contrast agent, Levovist® (SH U 508A; Schering, Berlin, Germany), consists of air-microbubbles and is commercially available in many countries.[19] But Levovist® visualizes the enhanced image by destroying the microbubbles, and hence it is not suitable for continuous examination. To visualize enhanced images without destroying the contrast agents, second-generation agents are being developed. Sonazoid was released in Japan and SonoVue or Definity are available in Western countries.[12,13,20,21] We believe that our study can also be performed with other second-generation contrast material, SonoVue or Definity, which would lead to the same results and considerations.

It is not practical to evaluate the vascularity of all tumors by USHA technique because the process would be invasive and relatively complicated, so we do not recommend it for routine examinations of liver tumors in future. Contrast-enhanced US and CT during angiography are well-established modalities and each has already provided abundant information. Specifically, US can generate minute pictures and CT during angiography can provide separate arterial and portal-venous perfusion images. The method used in our work seems to be intermediate between the two modalities and adapts information about drainage flow obtained with CT during angiography to the precise images obtained with US. We have empirically created some ablative margin with RFA to ensure that ablation of the tumor itself was complete, but the detection of corona enhancement on the US image taught us the drainage area for US-based local ablation therapy. When local ablation therapy such as RFA is used, the drainage area from the tumor should be included in the ablated area. Therefore, it should be remembered that the targeted ablation area must include the margin of the enhanced edge on ordinary contrasted US images. We hope our findings will be helpful for understanding the necessity of adequate ablative margins for curative treatments for HCC.

In conclusion, in this report we introduced new findings obtained by means of US during selective arteriography. Selective enhancement of the arterial flow enabled visualization of corona enhancement on US images, which would be helpful for identifying the drainage area for US-based local ablation therapy. The fact that mean width of corona enhancement was 6 mm may well explain the frequent local recurrence in cases without an ablative margin of at least 5 mm.

REFERENCES

1 Matsui O, Kadoya M, Suzuki M *et al.* Work in progress: dynamic sequential computed tomography during arterial portography in the detection of hepatic neoplasms. *Radiology* 1983; 146: 721–7.
2 Matsui O, Takashima T, Kadoya M *et al.* Dynamic computed tomography during arterial portography: the most sensitive examination for small hepatocellular carcinomas. *J Comput Assist Tomogr* 1985; 9: 19–24.
3 Chezmar JL, Bernardino ME, Kaufman SH, Nelson RC. Combined CT arterial portography and CT hepatic angiog-

raphy for evaluation of the hepatic resection candidate. *Radiology* 1993; 189: 407–10.
4 Ueda K, Matsui O, Kawamori Y *et al.* Hypervascular hepatocellular carcinoma: evaluation of hemodynamics with dynamic CT during hepatic arteriography. *Radiology* 1998; 206: 161–6.
5 Ueda K, Matsui O, Kawamori Y *et al.* Differentiation of hypervascular hepatic pseudolesions from hepatocellular carcinoma: value of single-level dynamic CT during hepatic arteriography. *J Comput Assist Tomogr* 1998; 22: 703–8.
6 Miyayama S, Matsui O, Ueda K *et al.* Hemodynamics of small hepatic focal nodular hyperplasia: evaluation with single-level dynamic CT during hepatic arteriography. *AJR Am J Roentgenol* 2000; 174: 1567–9.
7 Terayama N, Matsui O, Ueda K *et al.* Peritumoral rim enhancement of liver metastasis: hemodynamics observed on single-level dynamic CT during hepatic arteriography and histopathologic correlation. *J Comput Assist Tomogr* 2002; 26: 975–80.
8 Nishijima N, Kita R, Kawakami H *et al.* A case of an FNH-like hyperplastic nodule presenting ring enhancement in a peritumoral spared area on single-level dynamic CT during hapatic arteriography. *Kanzo* (in Japanese with English abstract) 2006, 47: 574–81.
9 Kita R, Nishijima N, Nakatsuji M *et al.* Corona enhancement may emerge via sinusoidal drainage pathways. *Kanzo* (in Japanese with English abstract) 2007, 48: 246–8.
10 Kita R, Nakatsuji M, Nishijima N *et al.* A case of focal nodular hyperplasia presenting corona enhancement on single-level dynamic CT during hepatic arteriography. *Nippon Shokakibyo Gakkai Zasshi* (in Japanese with English abstract) 2008, 105: 550–7.
11 Sakon M, Nagano H, Nakamori S *et al.* Intrahepatic recurrence of hepatocellular carcinoma after hepatectomy. Analysis based on tumor hemodynamics. *Arch Surg* 2002; 137: 94–9.
12 Watanabe R, Matsumura M, Chen CJ, Kaneda Y, Ishihara M, Fujimaki M. Gray-scale liver enhancement with Sonazoid (NC100100), a novel ultrasound contrast agent; detection of hepatic tumors in a rabbit model. *Biol Pharm Bull* 2003; 26: 1272–7.
13 Kudo M. New sonographic techniques for the diagnosis and treatment of hepatocellular carcinoma. *Hepatol Res* 2007; 37: S193–9.
14 Okusaka T, Okada S, Ueno H *et al.* Satellite lesions in patients with small hepatocellular carcinoma with reference to clinicopathologic features. *Cancer* 2002; 95: 1931–7.
15 Nakazawa T, Kokubu S, Shibuya A *et al.* Radiofrequency ablation of hepatocellular carcinoma: correlation between local tumor progression after ablation and ablation margin. *AJR Am J Roentgenol* 2007; 188: 480–8.
16 Ikeda K, Seki T, Umehara H *et al.* Clinicopathologic study of small hepatocellular carcinoma with microscopic satellite nodules to determine the extent of tumor ablation by local therapy. *Int J Oncol* 2007; 31: 485–91.
17 Nishijima N, Osaki Y, Kita R *et al.* Proposal of radicality grading as a criterion for therapeutic effectiveness of RFA against hepatocellular carcinoma in terms of local recurrence rate. *Kanzo* (in Japanese with English abstract) 2008, 49: 192–9.
18 Nakashima Y, Nakashima O, Tanaka M, Okuda K, Nakashima M, Kojiro M. Portal vein and intrahepatic micrometastasis in small hepatocellular carcinoma by gross type. *Hepatol Res* 2003; 26: 142–7.
19 Anqeli E, Carpanelli R, Crespi G, Zanello A, Sironi S, Del Maschio A. Efficacy of SH U 508A(Levovist) in color doppler ultrasonography of hepatocellular carcinoma vascularization. *Radiol Med* 1994; 87: 24–31.
20 Calliada F, Campani R, Bottinelli O, Bozzini A, Sommaruga MG. Ultrasound contrast agents: basic principles. *Eur J Radiol* 1998; 27: S157–160.
21 Wilson SR, Burns PN, Muradali D, Wilson JA, Lai X. Harmonic hepatic US with microbubble contrast agent: initial experience showing improved characterization of hemangioma, hepatocellular carcinoma, and metastasis. *Radiology* 2000; 215: 153–61.

Dynamics of Hepatitis B Virus Quasispecies in Association with Nucleos(t)ide Analogue Treatment Determined by Ultra-Deep Sequencing

Norihiro Nishijima[1], Hiroyuki Marusawa[1]*, Yoshihide Ueda[1], Ken Takahashi[1], Akihiro Nasu[1], Yukio Osaki[2], Tadayuki Kou[3], Shujiro Yazumi[3], Takeshi Fujiwara[4], Soken Tsuchiya[4], Kazuharu Shimizu[4], Shinji Uemoto[5], Tsutomu Chiba[1]

1 Department of Gastroenterology and Hepatology, Graduate School of Medicine, Kyoto University, Kyoto, Japan, **2** Department of Gastroenterology and Hepatology, Osaka Red Cross Hospital, Osaka, Japan, **3** Department of Gastroenterology and Hepatology, Tazuke Kofukai Medical Research Institute, Kitano Hospital, Osaka, Japan, **4** Department of Nanobio Drug Discovery, Graduate School of Pharmaceutical Sciences, Kyoto University, Kyoto, Japan, **5** Department of Surgery, Graduate School of Medicine, Kyoto University, Kyoto, Japan

Abstract

Background and Aims: Although the advent of ultra-deep sequencing technology allows for the analysis of heretofore-undetectable minor viral mutants, a limited amount of information is currently available regarding the clinical implications of hepatitis B virus (HBV) genomic heterogeneity.

Methods: To characterize the HBV genetic heterogeneity in association with anti-viral therapy, we performed ultra-deep sequencing of full-genome HBV in the liver and serum of 19 patients with chronic viral infection, including 14 therapy-naïve and 5 nucleos(t)ide analogue(NA)-treated cases.

Results: Most genomic changes observed in viral variants were single base substitutions and were widely distributed throughout the HBV genome. Four of eight (50%) chronic therapy-naïve HBeAg-negative patients showed a relatively low prevalence of the G1896A pre-core (pre-C) mutant in the liver tissues, suggesting that other mutations were involved in their HBeAg seroconversion. Interestingly, liver tissues in 4 of 5 (80%) of the chronic NA-treated anti-HBe-positive cases had extremely low levels of the G1896A pre-C mutant (0.0%, 0.0%, 0.1%, and 1.1%), suggesting the high sensitivity of the G1896A pre-C mutant to NA. Moreover, various abundances of clones resistant to NA were common in both the liver and serum of treatment-naïve patients, and the proportion of M204VI mutants resistant to lamivudine and entecavir expanded in response to entecavir treatment in the serum of 35.7% (5/14) of patients, suggesting the putative risk of developing drug resistance to NA.

Conclusion: Our findings illustrate the strong advantage of deep sequencing on viral genome as a tool for dissecting the pathophysiology of HBV infection.

Citation: Nishijima N, Marusawa H, Ueda Y, Takahashi K, Nasu A, et al. (2012) Dynamics of Hepatitis B Virus Quasispecies in Association with Nucleos(t)ide Analogue Treatment Determined by Ultra-Deep Sequencing. PLoS ONE 7(4): e35052. doi:10.1371/journal.pone.0035052

Editor: Antonio Bertoletti, Singapore Institute for Clinical Sciences, Singapore

Received November 17, 2011; **Accepted** March 8, 2012; **Published** April 16, 2012

Funding: This work was supported by JSPS Grant-in-aid for Scientific Research 21229009, 23390196, and Health and Labor Science Research Grants (H22-08) and Research on Hepatitis from the Ministry of Health, Labor and Welfare, Japan. (http://mhlw-grants.niph.go.jp/). The funders had no role in study design, data collection and analysis, decision to publish, or preparation of the manuscript.

Competing Interests: The authors have declared that no competing interests exist.

* E-mail: maru@kuhp.kyoto-u.ac.jp

Introduction

Hepatitis B virus (HBV) is a non-cytopathic DNA virus that infects approximately 350 million people worldwide and is a main cause of liver-related morbidity and mortality [1–3]. The absence of viral-encoded RNA-dependent DNA polymerase proofreading capacity coupled with the extremely high rate of HBV replication yields the potential to rapidly generate mutations at each nucleotide position within the entire genome [4]. Accordingly, a highly characteristic nature of HBV infection is the remarkable genetic heterogeneity at the inter- and intra- patient level. The latter case of variability as a population of closely-related but nonidentical genomes is referred to as viral quasispecies [5,6]. It is well recognized that such mutations may have important implications regarding the pathogenesis of viral disease. For example, in chronic infection, G to A point mutation at nucleotide (nt) 1896 in the pre-core (pre-C) region as well as A1762T and G1764A mutations in the core-promoter region are highly associated with HBeAg seroconversion that in general results in the low levels of viremia and consequent clinical cure [7 9]. In contrast, acute infection with the G1896A pre-C mutant represents a high risk for fulminant hepatic failure [10,11]. Although these facts clearly illustrate the clinical implications of certain viral mutation, increasing evidence strongly suggests that

the viral genetic heterogeneity is more complicated than previously thought [12,13].

The major goals of antiviral therapy in patients with HBV infection are to prevent the progression of liver disease and inhibit the development of hepatocellular carcinoma [14]. Oral nucleos(t)ide analogue (NA) have revolutionized the management of HBV infection, and five such antiviral drugs, including lamivudine, adefovir, entecavir, tenofovir, and telbivudine, are currently approved medications [15,16]. These agents are well-tolerated, very effective at suppressing viral replication, and safe, but one of the major problems of NA therapy is that long-term use of these drugs frequently causes the emergence of antiviral drug-resistant HBV due to substitutions at specific sites in the viral genome sequences, which often negates the benefits of therapy and is associated with hepatitis flares and death [16,17]. It is unclear whether viral clones with antiviral resistance emerge after the administration of antiviral therapy or widely preexist among treatment-naïve patients.

There has been a recent advance in DNA sequencing technology [18]. The ultra-deep sequencers allow for massively parallel amplification and detection of sequences of hundreds of thousands of individual molecules. We recently demonstrated the usefulness of ultra-deep sequencing technology to unveil the massive genetic heterogeneity of hepatitis C virus (HCV) in association with treatment response to antiviral therapy [19]. On the other hand, there are a few published studies in which this technology was used to characterize genetic HBV sequence variations [20–22]. Margeridon-Thermet et al reported that the 454 Life Science GS20 sequencing platform provided higher sensitivity for detecting drug-resistant HBV mutations in the serum of patients treated with nucleoside and nucleotide reverse-transcriptase inhibitors [20]. Solmone et al also reported the strong advantage conferred by the same platform to detect minor variants in the serum of patients with chronic HBV infection [21]. Although in these previous studies low-abundant drug-resistant variants were successfully detected, the analyses were focused on the reverse-transcriptase region of circulating HBV in the serum and thus the whole picture of HBV genetic heterogeneity as well as the *in vivo* dynamics of HBV drug resistant variants in response to anti-viral treatment remains to be clarified. Moreover, intrahepatic viral heterogeneity in patients that achieved the clearance of circulating HBV is largely unknown.

By taking the advantage of an abundance of genetic information obtained by utilizing the Illumina Genome Analyzer II (Illumina, San Diego, CA) as a platform of ultra-deep sequencing, we determined the whole HBV sequence in the liver and serum of patients with chronic HBV infection to evaluate viral quasispecies characteristics. Moreover, we investigated the prevalence of rare drug-resistant HBV variants as well as detailed dynamic changes in the viral genetic heterogeneity in association with NA administration. Based on the abundant genetic information obtained by ultra-deep sequencing, we clarified the precise prevalence of HBV clones with G1896A pre-C mutations in association with HBe serostatus in chronically infected patients with or without NA treatment. We also detected a variety of minor drug-resistant clones in treatment-naïve patients and their dynamic changes in response to entecavir administration, demonstrating the potential clinical significance of naturally-occurring drug-resistant mutations.

Materials and Methods

Ethics Statement

The Kyoto University ethics committee approved the study, and written informed consent for participation in this study was obtained from all patients. The study was conducted in accordance with the principles of the Declaration of Helsinki.

Patients

The liver tissues of 19 Japanese patients that underwent living-donor liver transplantation at Kyoto University due to HBV-related liver disease were available for viral genome analyses. These individuals included 13 men and 6 women, aged 41 to 69 years (median, 55.2 years) and all but one were infected with genotype C viruses. Participants comprised 19 patients with liver cirrhosis caused by chronic HBV infection, including 14 antiviral therapy-naïve cases (chronic-naïve cases) and 5 cases receiving NA treatment, with either lamivudine or entecavir (chronic-NA cases) (Table 1). Serum HBV DNA levels were significantly higher in chronic-naïve cases than in chronic NA cases (median serum HBV DNA levels were 5.6, and <2.6 log copies/ml, respectively, Table 1). Liver tissue samples were obtained at the time of transplantation, frozen immediately, and stored at $-80^{\circ}C$ until use. Serologic analyses of HBV markers, including hepatitis B surface antigen (HBsAg), antibodies to HBsAg, anti-HBc, HBeAg, and antibodies to HBeAg, were determined by enzyme immunoassay kits as described previously [23]. HBV DNA in the serum before transplantation was examined using a polymerase chain reaction (PCR) assay (Amplicor HBV Monitor, Roche, Branchburg, NJ). To examine the dynamics of viral quasispecies in response to anti-HBV therapy, paired serum samples of 14 treatment-naïve patients before and after administration of daily entecavir (0.5 mg/day) were subjected to further analyses on viral genome.

Direct population Sanger sequencing

DNA was extracted from the liver tissue and serum using a DNeasy Blood & Tissue Kit (Qiagen, Tokyo, Japan). To define the consensus reference sequences of HBV in each clinical specimen, all samples were first subjected to direct population Sanger sequencing using the Applied Biosystems 3500 Genetic Analyzer (Applied Biosystems, Foster City, CA). Oligonucleotide primers for the HBV genome were designed to specifically amplify whole viral sequences as two overlapping fragments using the sense primer 169_F and antisense primer 2847_R to yield a 2679-bp amplicon (amplicon 1), and the sense primer 685_F and antisense primer 443_R to yield a 2974-bp amplicon (amplicon 2; Table S1). HBV sequences were amplified using Phusion High-Fidelity DNA polymerase (FINZYMES, Espoo, Finland). All amplified PCR products were purified using the QIAquick Gel Extraction kit (Qiagen) after agarose gel electrophoresis and used for direct sequencing. The serum of a healthy HBV DNA-negative volunteer was used as a negative control.

Viral genome sequencing by massively-parallel sequencing

Massively-parallel sequencing with multiplexed tags was performed using the Illumina Genome Analyzer II as described [19]. The end-repair of DNA fragments, addition of adenine to the 3′ ends of DNA fragments, adaptor ligation, and PCR amplification by Illumina PCR primers were performed as described previously [24]. Briefly, the viral genome sequences were amplified by high-fidelity PCR using oligonucleotide primers as described above, sheared by nebulization using 32 psi N2 for 8 min, and then the sheared fragments were purified and concentrated using a QIAquick PCR purification Kit (Qiagen). Nucleotide overhangs resulting from fragmentation were then converted into blunt ends using T4 DNA polymerase and Klenow

Table 1. Characteristics of patients with chronic HBV infection analyzed in this study.

	Chronic-naïve (N = 14)	Chronic-NA (N = 5)
Age†	55.5 (41–69)	55.0 (49–68)
Sex (male/female)	9/5	4/1
Alanine aminotransaminase (IU/l)†	41 (10–74)	30 (15–65)
Total bilirubin (mg/dl)†	0.9 (0.5–31.1)	1.7 (0.6–4.5)
Platelet count ($\times 10^4$/mm^3)†	12.7 (3.3–27.6)	5.1 (3.6–11.3)
HBV genotype		
B	1	0
C	13	5
Viral load (log copies /ml)†	5.6 (<2.6–8.8)*	<2.6 (<2.6–5.3)*
HBe-serostatus (HBeAg+/HBeAb+)	8/6	0/5
Fibrosis		
F0–F2	6	0
F3–F4	8	5
Activity		
A0–A1	7	3
A2–A3	7	2

†Values are median (range).
*P = 0.042.
doi:10.1371/journal.pone.0035052.t001

enzymes, followed by the addition of terminal 3′ A-residues. An adaptor containing unique 6-bp tags, such as "ATCACG" and "CGATGT" (Multiplexing Sample Preparation Oligonucleotide Kit, Illumina), was then ligated to each fragment using DNA ligase. We then performed agarose gel electrophoresis of adaptor-ligated DNAs and excised bands from the gel to produce libraries with insert sizes ranging from 200 to 350 bp. These libraries were amplified independently using a minimal PCR amplification step of 18 cycles by Illumina PCR primers with Phusion High-Fidelity DNA polymerase. The DNA fragments were then purified with a MinElute PCR Purification Kit (Qiagen), followed by quantification using the NanoDrop 2000C (Thermo Fisher Scientific, Waltham, MA) to make a working concentration of 10 nM. Cluster generation and sequencing was performed for 64 cycles on the Illumina Genome Analyzer II according to the manufacturer's instructions. The obtained images were analyzed and base-called using GA pipeline software version 1.4 with the default settings provided by Illumina.

Genome Analyzer sequence data analysis

Using the high performance alignment software "NextGene" (SoftGenetics, State College, PA), the 64 base-pair reads obtained from the Genome Analyzer II were aligned with the reference sequences of 3215 bp that were determined by direct population Sanger sequencing of each clinical specimen. Reads with 90% or more bases matching a particular position of the reference sequences were aligned. Furthermore, two quality filters were used for sequencing reads: the reads with a median quality score of more than 30 and no more than 3 uncalled nucleotides were allowed anywhere in the 64 bases. Only sequences that passed the quality filters, rather than raw sequences, were analyzed and each position of the viral genome was assigned a coverage depth, representing the number of times the nucleotide position was sequenced.

Allele-specific quantitative real-time PCR and semiquantitative PCR to determine the relative proportion of G1896A pre-C mutant

To determine the relative proportion of the G1896A pre-C mutant, allele-specific quantitative real-time PCR was performed based on the previously described method [25,26]. Oligonucleotide primers were designed individually to amplify the pre-C region of wild-type and the G1896A pre-C mutant HBV. Three primers were used for this protocol, two allele-specific sense primers, 1896WT_F (for wild-type) and 1896MT_F (for the G1896A pre-C mutant), and one common antisense primer, 2037_R (Table S1). Quantification of wild-type and the G1896A pre-C mutant was individually performed by real-time PCR using a Light Cycler 480 and Fast Start Universal SYBR Master (Roche, Mannheim, Germany) [27]. The relative proportion of the G1896A pre-C mutant was determined to calculate the G1896A pre-C mutant/total HBV ratios. Performance of this assay was tested using mixtures of two previously described plasmids, pcDNA3-HBV-wt#1 and pcDNA3-HBV-G1896A pre-C mutant [28]. Semiquantitative PCR was performed using primers described above, then agarose gel electrophoresis was performed.

Statistical analysis

Results are expressed as mean or median, and range. Pretreatment values were compared using the Mann-Whitney U-test or the Kruskal Wallis H-test. P values less than 0.05 were considered statistically significant.

The viral quasispecies characteristics were evaluated by analyzing the genetic complexity based on the number of different sequences present in the population. Genetic complexity for each site was determined by calculating the Shannon entropy using the following formula:

$$Sn = -\frac{\sum_{i=1}^{n} fi(lnfi)}{N}$$

where n is the number of different species identified, fi is the observed frequency of a particular variant in the quasispecies, and N is the total number of clones analyzed [12,13]. The mean viral complexity in each sample was determined by calculating the total amounts of the Shannon entropy at each nucleotide position divided by the total nucleotide number (e.g., 3215 bases) of each HBV genome sequence.

Nucleotide sequence accession number

All sequence reads have been deposit in DNA Data Bank of Japan Sequence Read Archive (http://www.ddbj.nig.ac.jp/index-e.html) under accession number DRA000435.

Results

Validation of multiplex ultra-deep sequencing of the HBV genome

To differentiate true mutations from sequencing errors in the determined sequences, we first generated viral sequence data from the expression plasmid, pcDNA3-HBV-wt#1, encoding wild-type genotype C HBV genome sequences [28]. For this purpose, we determined the PCR-amplified HBV sequences derived from the expression plasmid using high-fidelity Taq polymerase to take the PCR-induced errors as well as sequencing errors into consideration. Viral sequences determined by the conventional Sanger method were used as reference sequences for aligning the amplicons obtained by ultra-deep sequencing. Three repeated ultra-deep sequencing generated a mean of 77,663 filtered reads, corresponding to a mean coverage of 38,234 fold at each nucleotide site (Table S2). Errors comprised insertions (0.00003%), deletions (0.00135%), and nucleotide mismatches (0.037%). The mean overall error rate was 0.034% (distribution of per-nucleotide error rate ranged from 0 to 0.13%) for the three control experiments, reflecting the error introduced by high-fidelity PCR amplification and by multiplex ultra-deep sequencing that remained after filtering out problematic sequences. We also confirmed that multiplex ultra-deep sequencing with and without the high-fidelity PCR amplification with HBV-specific primer sets showed no significant differences in the error rates on the viral sequence data (mean error rate 0.034% vs 0.043%). Accordingly, we defined the cut-off value in its current platform as 0.3%, a value nearly 1 log above the mean overall error rate.

Next, we performed additional control experiments to verify the detectability of the low abundant mutations that presented at a frequency of less than 0.3%. For this purpose, we introduced expression plasmids with a single-point mutation within that encoding a wild-type viral sequence with a ratio of 1:1000 and assessed the sensitivity and accuracy of quantification using high-fidelity PCR amplification followed by multiplex ultra-deep sequencing in association with the different coverage numbers (Table S3). Repeated control experiments revealed that the threshold for detecting low-abundant mutations at an input ratio of 0.10% among the wild-type sequences ranged between 0.11% and 0.24%, indicating that there was no significant difference in the detection rate or error rates under the different coverage conditions. Based on these results, the accuracy of ultra-deep sequencing in its current platform for detecting low-level viral mutations was considered to be greater than 0.30%.

Viral complexity of the HBV quasispecies in association with clinical status

To clarify HBV quasispecies in association with clinical status, we performed multiplex ultra-deep sequencing and determined the HBV full-genome sequences in the liver and serum with chronic HBV infection. First, we compared the sequences of the viral genome determined in the liver tissue with those in the serum and found no significant differences in the viral population between the liver and serum of the same individual. Indeed, the pattern and distribution of genetic heterogeneity of the viral nucleotide sequences in the liver tissue were similar to those observed in the serum of the same patient (Figure S1), suggesting that a similar pattern of viral heterogeneity was maintained in the liver and serum of patients with chronic HBV infection.

Next, we compared the viral heterogeneity in the liver of chronic-naïve and chronic-NA cases. A mean of 5,962,996 bp nucleotides in chronic-naïve cases and 4,866,783 bp nucleotides in chronic-NA cases were mapped onto the reference sequences, and an overall average coverage depth of 1,855 and 1.514 was achieved for each nucleotide site of the HBV sequences, respectively (Table 2). The frequencies of mutated positions and altered sequence variations detected in each viral genomic region are summarized in Table 2. The overall mutation frequency of the total viral genomic sequences was determined to be 0.87% in chronic-naïve cases and 0.69% in chronic-NA cases. Most genomic changes observed in viral variants were single base substitutions, and the genetic heterogeneity of the viral nucleotide sequences was equally observed throughout the individual viral genetic regions, including the pre-surface (preS), S, pre-core~core (preC-C), and X (Table 2). Consistent with the findings obtained from the viral mutation analyses, the overall viral complexity determined by the Shannon entropy value was 0.047 in chronic-naïve and 0.036 in chronic-NA cases, and the viral complexity was equally observed throughout the individual viral genetic region (Figure 1A). Among chronic-naïve cases, we observed no significant differences in the viral complexity in HBV DNA level, age, or degree of fibrosis (Figure 1B).

High sensitivity of the G1896A pre-C mutant to nucleos(t)ide analogues

Emergence of G1896A mutation in the pre-C region, and A1762T and G1764A mutations in the core-promoter region is well known to be associated with HBe-seroconversion [7–9]. We then evaluated the prevalence of these three mutations in the chronically HBV-infected liver, in association with HBe serologic status and the NA treatment history. In chronic-naive cases, 6 and 8 patients showed the pre- and post- HBeAg seroconversion status, respectively (Table 3). The mean prevalence of the G1896A pre-C mutant in HBeAg-positive cases was lower than that in the HBeAg-negative cases (27.4% and 46.5%, respectively). Importantly, however, 4 of 8 HBeAg-negative cases showed a relatively low prevalence of the G1896A pre-C mutant (Liver #8, #12, #13, #14), and all but one case (Liver #10) showed a high prevalence of the A1762T and G1764A mutations, irrespective of HBe serologic status and NA treatment history (Table 3). These findings suggested that other mutations except G1896A, A1762T and G1764A were also involved in the HBeAg seroconversion status. Notably, liver tissues of all but one (Liver #17) chronic-NA cases showed extremely low levels of the G1896A pre-C mutant (0.0, 0.0, 0.1, and 1.1%), suggesting the high sensitivity of the G1896A pre-C mutant to NA (Table 3).

To confirm the difference of the sensitivity to NA between the wild-type and the G1896A pre-C mutant, we examined the dynamic changes of the relative proportion of the G1896A pre-C mutant in the serum of 14 treatment-naïve patients before and after entecavir administration. Consistent with the findings obtained by ultra-deep sequencing, quantitative real-time PCR revealed that entecavir administration significantly reduced the proportion of the G1896A pre-C mutant in 13 of 14 cases (92.9%)

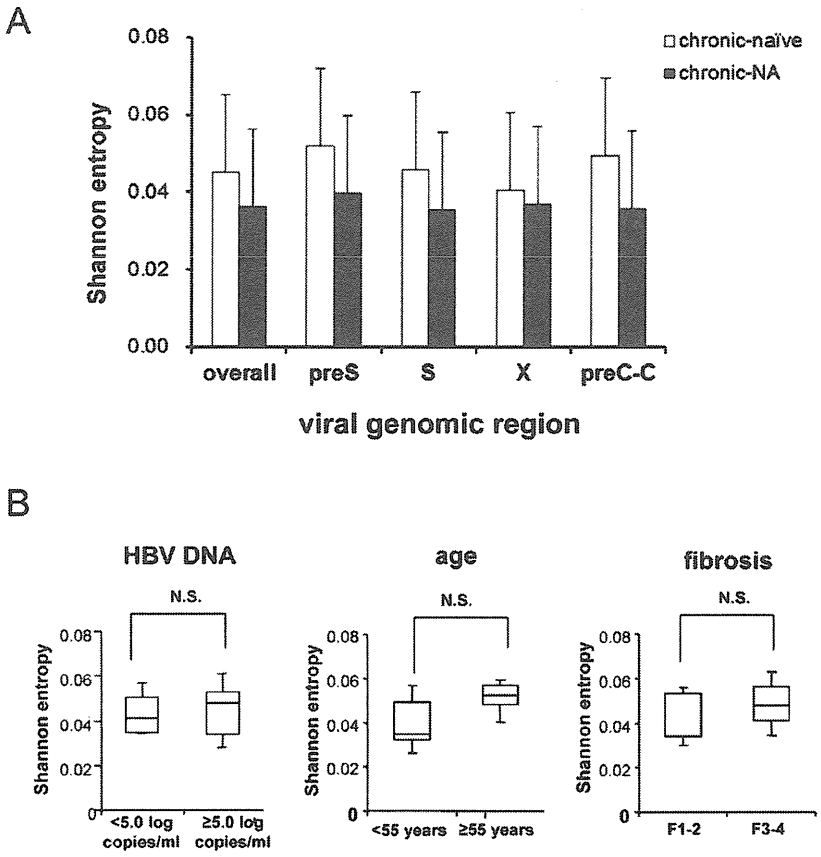

Figure 1. Viral complexity of the HBV quasispecies in association with clinical status. (A) The Shannon entropy values for each viral genomic region were determined in the liver of chronic-naïve and chronic-NA cases. (B) Among the chronic-naïve cases, the Shannon entropy values are shown for patients with serum HBV DNA levels less than 5.0 log copies/ml (<5.0) and greater than 5.0 log copies/ml (≥5.0) (left panel), patients under the age of 55 years (<55) and over the age of 55 (≥55) (middle panel), and patients with low (F1–2) and high (F3–4) liver fibrosis levels (right panel). preS: pre-surface, preC-C: precore~core N.S.: not significant.
doi:10.1371/journal.pone.0035052.g001

Table 2. The frequency of mutation rate and the Shannon entropy in each viral genome region.

	Liver	
	Chronic-naïve (N = 14)	Chronic-NA (N = 5)
Average aligned reads	93,172	76,043
Average aligned nucleotides	5,962,996	4,866,783
Average coverage	1,855	1,514
Mutation rate (%)		
Overall	0.87	0.69
preS	0.92	0.81
S	0.96	0.71
preC-C	1.05	0.72
X	0.63	0.61
Shannon entropy	0.047	0.036

Mutation rate (%): the ratio of total different nucleotides from the reference sequence to total aligned nucleotides.
preS: pre-surface, preC-C: pre-core~core.
doi:10.1371/journal.pone.0035052.t002

irrespective of their HBeAg serostatus, while the G1896A pre-C mutant were detectable in substantial proportion before treatment in all cases (Figure 2A, 2B and 2C; $p = 0.001$). These results further support the findings that HBV clones comprising the G1896A mutation were more sensitive to NA than those with wild-type sequences.

Prevalence of drug-resistant HBV clones in the liver of treatment-naïve patients

Increasing evidence suggests that drug-resistant viral mutants can be detected in the serum of treatment-naïve patients with chronic HBV infection [20,21]. Thus, we next determined the actual prevalence of spontaneously-developed drug-resistant mutants in chronically-infected liver of treatment-naïve patients to evaluate whether NA treatment potentiates the expansion of drug-resistant clones. The drug-resistant mutations examined included two mutations resistant to lamivudine and entecavir, four mutations resistant to entecavir, and three mutations resistant to adefovir [16,17]. Based on the detection rate of the low-level viral clones determined by the control experiments, we identified the drug-resistant mutants present in each specimen at a frequency of more than 0.3% among the total viral clones. Based on these criteria, at least one resistant mutation was detected in the liver of all of the chronic-naïve cases with chronic HBV infection (Table 4).

Table 3. The prevalence of G1896A mutation in the pre-C region, and A1762T and G1764A mutations in the core-promoter region in the liver of patients chronically infected with HBV.

			Mutation Frequency					
	HBeAg/HBeAb	NA (duration of treatment)	G1896A (Pre C)		A1762T (CP)		G1764A (CP)	
Chronic-naive								
Liver #1	+/−	-	640/1652	(38.7)	1647/1941	(84.9)	1683/1979	(85.0)
Liver #2	+/−	-	9/596	(1.5)	682/687	(99.3)	683/689	(99.1)
Liver #3	+/−	-	273/672	(40.6)	767/769	(99.7)	757/760	(99.6)
Liver #4	+/−	-	204/701	(29.1)	610/625	(97.6)	602/621	(96.9)
Liver #5	+/−	-	27/152	(17.8)	249/250	(99.6)	245/248	(98.8)
Liver #6	+/−	-	228/621	(36.7)	727/729	(99.7)	743/744	(99.9)
Liver #7	−/+	-	740/1193	(62.0)	1908/1913	(99.7)	1888/1913	(98.7)
Liver #8	−/+	-	111/1892	(5.9)	2321/2325	(99.8)	2335/2339	(99.8)
Liver #9	−/+	-	10935/10944	(99.9)	12019/12032	(99.9)	12163/12170	(99.9)
Liver #10	−/+	-	4554/4593	(99.2)	1/5191	(0)	4/5188	(0.1)
Liver #11	−/+	-	811/921	(88.1)	1234/1236	(99.8)	1226/1228	(99.8)
Liver #12	−/+	-	93/1265	(7.4)	1234/1234	(100)	1228/1229	(99.9)
Liver #13	−/+	-	83/877	(9.5)	1465/1529	(95.8)	1485/1549	(95.9)
Liver #14	−/+	-	0/717	(0)	1078/1410	(76.5)	1089/1414	(77.0)
Chronic-NA								
Liver #15	−/+	LAM (156w)	0/390	(0)	441/453	(97.4)	435/448	(97.1)
Liver #16	−/+	ETV (1w)	0/1399	(0)	1624/1632	(99.5)	1625/1630	(99.7)
Liver #17	−/+	LAM (144w)	345/816	(42.3)	988/991	(99.7)	994/994	(100)
Liver #18	−/+	LAM (98w)	2/3963	(0.1)	1015/1188	(85.4)	1190/1194	(99.7)
Liver #19	−/+	LAM (11w)	48/4214	(1.1)	3438/3456	(99.5)	3446/3462	(99.5)

Values in parenthesis show mutation frequency (%): the ratio of total mutant clones to total aligned coverage at each nucleotide sites.
NA: nucleotide analogue, pre C: precore, CP: core promoter, LAM: lamivudine, ETV: entecavir.
doi:10.1371/journal.pone.0035052.t003

The prevalence of the 9 drug-resistant mutations detected by ultra-deep sequencing in 14 chronic-naïve cases ranged from 0.3% to 30.0%, indicating that the proportion of resistant mutations substantially differed in each case. The most commonly detected mutation was M204VI (9 cases) and M250VI (11 cases), which were resistant to lamivudine and entecavir, and entecavir, respectively. Other mutations resistant to adefovir were detected in 7 (50.0%) and 3 (21.4%) cases at A181TV and N236T, respectively (Table 4).

Nine (64.2%) chronic-naïve cases possessed the M204VI mutants in their liver tissues and the proportion of mutant clones among the totally infected viruses ranged from 0.3% to 1.1% among the M204VI mutant-positive patients. In chronic-NA cases, 4 of 5 (80.0%) liver tissues harbored the M204VI mutants with the proportion among the totally infected viruses ranging from 0.4% to 18.7% (Table 4), while the mean serum HBV DNA was suppressed below 2.6 log copies/ml (Table 1). These results suggest that the mutant HBV clones comprising various drug-resistant mutations could latently exist even in the liver of NA treatment-naïve cases.

Expansion of drug-resistant HBV clones harboring M240VI mutations in response to NA administration

To clarify the risk of latent expansion of drug-resistant mutations due to NA treatment, we next examined the early dynamic changes of the prevalence of M204VI mutants in the serum of treatment-naïve patients in response to entecavir treatment. Ultra-deep sequencing provided a mean 40,791- and 38,823-fold coverage of readings, which were mapped to the M204VI nucleotide position at the YMDD sites of each reference sequence in patients before and after entecavir treatment.

Five of 14 (35.7%) patients harbored the M204VI mutations prior to entecavir treatment. Although the serum HBV DNA levels were significantly reduced in response to entecavir in all cases, the M204VI mutant clones were detected in 9 cases (64.3%) after entecavir administration (Table 5). Notably, one patient (Serum #3) who harbored the M240VI mutant clones at baseline had a relatively large expansion of drug-resistant clones among the total viral population in a time-dependent manner in response to entecavir treatment (Table 5). Similarly, M240VI mutant clones became detectable after entecavir administration in four patients (Serum #1, #7, #12, #13) that harbored no resistant mutants at baseline (Table 5). We found no correlation between the degree of the increase in the relative prevalence of M204VI mutant clones and that of the reduction in serum HBV DNA levels. Although only a limited number of patients exhibited a substantial increase in M204VI mutant clones after administration of anti-viral therapy, our findings might suggest that entecavir treatment latently causes selective survival of drug-resistant mutants in treatment naïve patients with chronic HBV infection.

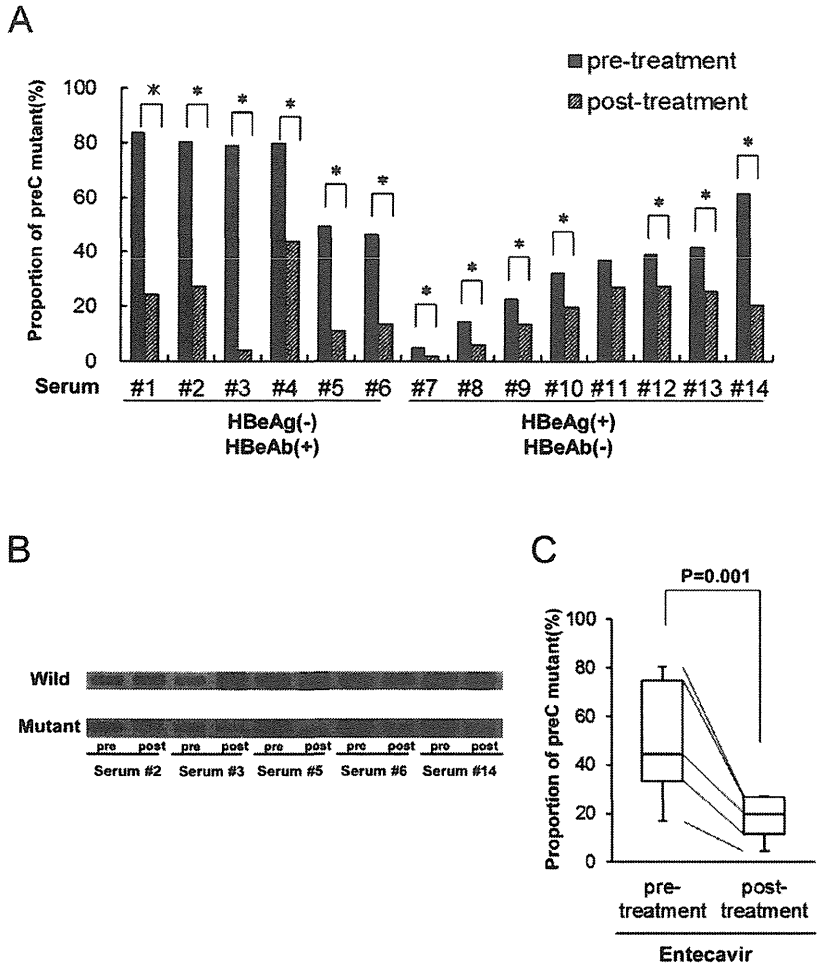

Figure 2. The reduction in the relative proportion of the G1896A pre-C mutant clones after entecavir administration. (A) The relative proportion of the G1896A pre-C mutant was determined in the serum of treatment-naïve patients pre- and post-entecavir administration using quantitative real-time PCR. Serum #1~6 were HBeAg-negative and HBeAb-positive, and Serum #7~14 were HBeAg-positive and HBeAb-negative before treatment. *: $p<0.05$ (B) Semiquantitative PCR analysis was performed using primers specific to the wild-type (upper panel) or G1896A pre-C mutant (lower panel) pre- and post-entecavir administration. A representative result from 5 cases is shown. (C) The relative proportion of the G1896A pre-C mutant was compared in 14 treatment-naïve patients between pre- and post-entecavir administration.
doi:10.1371/journal.pone.0035052.g002

Discussion

Direct population sequencing is the most common method for detecting viral mutations [29]. Conventional sequencing techniques, however, are not efficient for evaluating large amounts of genetic information of the viruses. Newly developed ultra-deep sequencing technology have revolutionized genomic analyses, allowing for studies of the dynamics of viral quasispecies as well as rare genetic variants of the viruses that cannot be detected using standard direct population sequencing techniques [30,31]. The sensitivity of ultra-deep sequencing analysis is primarily limited by errors introduced during PCR amplification and the sequencing reaction, thus it is a challenge to distinguish rare variants from sequencing artifacts. In the present study, we optimized the ultra-deep sequencing with a multiplex-tagging method and reproducibly detected variants within HBV quasispecies that were as rare as 0.3%. Based on this ultra-deep sequencing platform, we determined the abundant genetic heterogeneity of HBV at the intra- and inter-individual levels.

Because of its ability to handle abundant viral genome information, ultra-deep sequencing allowed us to evaluate low-abundant virus variants of patients with chronic HBV infection in detail. It is widely accepted that HBe seroconversion is highly associated with the emergence of G1896A pre-C and/or A1762T and G1764A core promoter mutant clones [7–9]. Unexpectedly, however, our results showed a diverse range of G1896A frequency (0–99.9%) in HBeAg-negative subjects and a high prevalence of core promoter mutations, irrespective of HBe serostatus. Consistent with our observation, previous studies utilizing conventional sequencing methods reported that the frequency of the G1896A pre-C mutant ranged from 12% to 85% [32]. All but one patient (Liver #10) showing a predominance of A1762T and G1764A were infected with genotype C, while patient#10 was infected with genotype B. Because A1762T and G1764A are reported to be significantly more frequent in genotype C [33], the difference in the prevalence of A1762T and G1764A in our study might be a reflection of the viral HBV genotype rather than HBe serostatus. Further investigation of the actual prevalence of these mutations